Available online at www.sciencedirect.com
SCIENCE DIRECT®
Microporous and Mesoporous Materials 75 (2004) 89–100
MICROPOROUS AND MESOPOROUS MATERIALS
www.elsevier.com/locate/micromeso

Structural, compositional and acidic characteristics of nanosized amorphous or partially crystalline ZSM-5 zeolite-based materials

Kostas S. Triantafyllidis [a,*], Lori Nalbandian [a], Pantelis N. Trikalitis [b], Athanasios K. Ladavos [c], Thomas Mavromoustakos [d], Christakis P. Nicolaides [e,*,1]

[a] *Chemical Process Engineering Research Institute—CPERI, Centre for Research and Technology Hellas—CERTH, 6th km. Harilaou-Thermi Road, P.O. Box 361, 57001 Thessaloniki, Greece*
[b] *Department of Chemistry, School of Sciences, University of Crete, P.O. Box 1470, Heraklion 71409, Crete, Greece*
[c] *Department of Farm Organization and Management, School of Natural Resource and Enterprise Management, University of Ioannina, Agrinio 30100, Greece*
[d] *Institute of Organic and Pharmaceutical Chemistry, National Hellenic Research Foundation, Vas. Constantinou Av. 48, Athens 11635, Greece*
[e] *Molecular Sciences Institute, School of Chemistry, University of the Witwatersrand, P.O. WITS, Johannesburg 2050, South Africa*

Received 18 July 2003; received in revised form 23 June 2004; accepted 13 July 2004
Available online 11 September 2004

Abstract

Partially crystalline and X-ray amorphous ZSM-5 zeolite-based aluminosilicates have been synthesized and thoroughly characterized by chemical analysis, XRD, FT-IR, solid state MAS NMR, N_2 adsorption, TEM, NH_3-TPD and isopropanol dehydration as the catalytic test reaction. The X-ray amorphous and low-crystallinity samples were hydrothermally synthesized at temperatures as low as 25 °C and consisted of nanosized well-formed particles of almost spherical shape and with dimensions of about 20–30 nm. These samples exhibited very low microporosity and remarkably high meso/macropore volume (pore diameters $\geqslant$30 nm) and/or high external surface area. The first Bragg peaks were observed in the XRD patterns of the samples synthesized at 90 °C and their position on the 2θ-axis was the same as those of a reference highly crystalline ZSM-5 zeolite sample. The particle/crystal size and microporosity of the partially crystalline materials increased with increasing hydrothermal synthesis temperature and % relative XRD crystallinity. Incorporation of aluminum in the ZSM-5 zeolitic framework was significantly enhanced at higher relative crystallinities, i.e. >60%. The X-ray amorphous aluminosilicates possessed tetrahedral aluminum atoms which were more zeolitic in character and induced a higher number of acidic framework hydroxyls (Brønsted acid sites), as compared to those found in a conventional silica–alumina.

Keywords: Nanosized zeolites; Partially crystalline ZSM-5; Framework aluminum; Acidity; Porosity

1. Introduction

The activity and product selectivity of acidic zeolite catalysts depend strongly on the number, strength and nature of the acid sites present [1,2], and on the shape and size of the micropores which can induce different shape-selectivity effects on the product distribution [3]. In addition, the crystal/particle size and morphology

* Corresponding authors. Addresses: CPERI/CERTH, P.O. Box 361, 57001 Thessaloniki, Greece. Tel.: +30 2310 498 310; fax: +30 2310 498 380 (K.S. Triantafyllidis), Sasol Technology, R&D Division, P.O. Box 1, Sasolburg 1947, South Africa. Tel.: +27 16 960 4318; fax: +27 11 522 4142 (C.P. Nicolaides).
E-mail addresses: ktrianta@cperi.certh.gr (K.S. Triantafyllidis), chris.nicolaides@sasol.com (C.P. Nicolaides).
[1] Present address: Sasol Technology, R&D Division, P.O. Box 1, Sasolburg 1947, South Africa.

1387-1811/$ - see front matter © 2004 Elsevier Inc. All rights reserved.
doi:10.1016/j.micromeso.2004.07.016

can also influence their catalytic performance. Smaller crystals/particles offer shorter intracrystalline diffusion paths for the reactants and products, and possess a higher number of external active sites compared to larger crystals [4–6]. It can also be stated that an appropriate balance between the active sites on the outer surface of the crystals and those in the intracrystalline micropore network may provide effective shape-selective catalysts for the conversion of hydrocarbon feedstocks with a broad range of sizes and molecular weights (e.g. vacuum gas–oil).

A significant research effort over the past few years has been devoted to the synthesis of zeolitic nanocrystals/nanoparticles, mainly for catalytic applications. For instance, the synthesis and characterization of nanocrystalline zeolite Beta with Si/Al ratio as low as 7–8 and crystal size of ~10 nm was recently reported by Camblor et al. [7]. From a catalytic point of view, the nanosized zeolite Beta can be very promising, since apart from the very small crystal size and the relatively high crystallinity, it also exhibits a large mesoporous volume (due to the interparticle space) with a narrow distribution of pore diameters, similar to that of the MCM-type materials. The advantage of this combination is related to the ability to convert relatively large hydrocarbon molecules that can diffuse through the interparticle mesopores and react on the external acid sites of the small zeolitic crystallites. The synthesis of other nanosized crystalline zeolites such as ZSM-5 and zeolite L has also been reported [8–11].

In an effort to reduce the crystal size of ZSM-5 zeolite by using shorter hydrothermal synthesis times, Jacobs et al. [12] in the early 1980's described the synthesis of X-ray amorphous zeolites which contained small crystallites of less than 8 nm in size within an amorphous matrix. This was shown by the presence of the infrared band at ~550 cm^{-1}, which has been assigned to the five-membered ring of the pentasil zeolite structure [13,14]. Furthermore, it was reported that the hydroconversion activity and product selectivity of the Pt-modified nanosized precursor zeolitic materials was comparable to those of the crystalline Pt/ZSM-5 zeolite catalyst. Through a different approach, Van Bekkum and co-workers [15] synthesized nanosized MFI-type crystallites of approximately 3 nm (as characterized by XRD, TEM and ^{13}C NMR analysis of the as-synthesized samples) in their attempts to re-crystallize the walls of a typical mesoporous MCM-41 aluminosilicate material by the use of tetrapropylammonium (TPA) hydroxide as the organic template molecule.

The formation of nanosized precursor species and the subsequent crystal growth during the crystallization of the MFI-type zeolite has recently been the subject of in-depth investigations using advanced in situ and ex situ characterization techniques, such as X-ray diffraction in Debye–Scherrer configuration, small-angle X-ray or neutron scattering (SAXS or SANS), laser-light scattering, TEM, IR, MAS NMR, etc. [13,16–21]. Small highly siliceous species with dimensions 3–5 nm, occluding tetrapropylammonium organic cations as structure directing agents, are formed even at room temperature. These "nanoblocks" or "nanoslabs" as they were named, can further condense and polymerize to form larger crystallites/particles upon heating, while the powdered products of these species show characteristics of the MFI structure that can be identified by IR, X-ray scattering and NMR spectroscopy. In a more recent work [22], related to the synthesis of MCM-type mesoporous materials, protozeolitic nanoclusters or "zeolite seeds", which were X-ray amorphous but contained zeolitic subunits, were utilized for the assembly of mesostructured aluminosilicates (MSU-S) with hydrothermal stability approaching that of the corresponding zeolites that they nucleate (i.e. Y, ZSM-5, Beta).

Recently, Nicolaides et al. [23–25] reported the synthesis and catalytic evaluation of X-ray amorphous or partially crystalline zeolitic materials (NAS materials) that have been prepared following a typical hydrothermal TPA-templated synthesis of the zeolite ZSM-5 but using lower synthesis temperatures (i.e. 25–140 °C). A linear correlation was found between the *n*-hexane cracking activity and the number of strong Brønsted acid sites (as determined by NH_3-microcalorimetry) of the proton-exchanged samples. For the samples with XRD relative crystallinities <30%, the number of strong acid sites and the *n*-hexane cracking activity were found to be disproportionately low, and both become significantly higher only at crystallinity levels higher than 30% [25]. Most interestingly, the 2–3% crystalline sample produced the highest yield of isobutene in the skeletal isomerization of 1-butene, whereas an increase in the relative crystallinity of the materials led to higher conversion values and to significantly lower selectivities to isobutene [23]. In a subsequent study, the zinc- and gallium-doped ZSM-5 zeolite-based samples with relative crystallinities between 50% and 85% were found to be the more active and selective catalysts for the conversion of propane into benzene, toluene and xylene [24].

In the present work we have focused on the characterization of these X-ray amorphous or partially crystalline ZSM-5 zeolite-based materials (NAS materials) in terms of their composition, structure, crystal/particle morphology and acidic properties as a function of % relative crystallinity. Their compositional and acidic characteristics were further correlated with their catalytic activity in the dehydration of isopropanol. Although these materials appear similar in composition and relative crystallinity to mildly or severely hydrothermally dealuminated ZSM-5 zeolites [26], they showed distinct structural, morphological and acidic properties as a consequence of the lower hydrothermal synthesis temperatures that were employed.

2. Experimental section

2.1. Preparation of the ZSM-5 zeolite-based materials

The synthesis of the amorphous or partially crystalline zeolitic materials (denoted as NAS) has been described in detail before [23]. A set of ZSM-5 zeolite-based samples with different degrees of crystallinity was prepared for this study by varying the temperature of the hydrothermal synthesis procedure from 25 to 150 °C. For all samples, the Si/Al ratio of the synthesis gel was 35 and the crystallization time was 72 h (under autogenous pressure). The number appearing after "NAS" indicates the temperature at which the synthesis was carried out. A highly crystalline commercial ZSM-5 zeolite (denoted as ZSM-5/R) with Si/Al ratio of ~28 was used as reference material. An amorphous silica–alumina sample (denoted as AmSiAl) was also synthesized by the co-precipitation of a waterglass solution with freshly prepared sodium aluminate solution using nitric acid (Si/Al ratio of the gel was 35) [27]. All the as-synthesized NAS solids were calcined in air at 630 °C for 3 h and were then ion-exchanged with 1 M NH_4Cl solution (using 10 ml solution per gram of solid) three times at room temperature, followed by washing with de-ionized water and drying at room temperature. The sodium content of the NAS-samples that were synthesized at low hydrothermal temperatures (i.e. 25, 50 and 90 °C) was relatively high (~0.5–1.4 wt.% Na) after the above-mentioned ion-exchange treatment. Samples NAS-25 and NAS-50 were therefore ion-exchanged one more time and sample NAS-90 two more times, with 1 M NH_4Cl solution, using 50 ml solution per gram of solid at 60 °C for 24 h. The NH_4^+-exchanged samples were calcined in air at 550 °C for 3 h in order to prepare the H^+-form of the materials and were stored over saturated $MgCl_2$ solution to equilibrate with water vapor before characterization and testing.

2.2. Composition, structure and morphology characterization

The total Al and Na content of the samples was determined by Atomic Emission Spectroscopy (ICP-AES) (Plasma 40, Perkin Elmer instrument) and the water content (up to 800 °C) by thermogravimetric analysis (SDT 2960, TA Instruments). The % SiO_2 was determined from the difference $\{100 - (\%Al_2O_3 + \%Na_2O + \%H_2O)\}$ and the total Si/Al ratio was then calculated from the relative amounts of the oxides.

The X-ray powder diffraction (XRD) patterns were obtained using a Siemens D-500 automated diffractometer (Cu Kα radiation, $\lambda = 1.5418$ Å), in the 2θ range of 5–45 deg and at a scanning rate of 1 deg min^{-1}. The relative crystallinity of the NAS samples was determined by comparing the sum of the intensities of the three dominant XRD peaks between 22 and 25 deg 2θ (i.e. those at ~23.02, 23.80 and 24.30 2θ) with the sum of the above peaks of the reference ZSM-5/R sample [23].

Mid-infrared (IR) spectra were recorded at 2 cm^{-1} resolution on a Perkin Elmer 1650 FT-IR spectrometer using KBr pellets (1 wt% zeolite in KBr matrix).

High-resolution solid state ^{29}Si MAS NMR spectra were recorded on a Varian 400 VRX spectrometer working at 79.5 MHz, with a pulse width of 6 μs, a pulse delay of 400 s, a spinning frequency of 4 kHz and 1,000 scans. The ^{27}Al MAS NMR experiments were run on a Varian Infinity plus AS400 spectrometer at 104.26 MHz, with a pulse width of 0.5 μs, a radiofrequency field strength of 50 G, a pulse delay of 0.5 s, a spinning rate of 4 kHz and 85,000 scans. ^{29}Si shifts were externally referenced to talc (−98.1 ppm relative to tetramethylsilane), while a 1 M aqueous $Al(NO_3)_3$ solution was used as reference for ^{27}Al.

Specific surface area (SSA) and porosity characteristics of the samples were determined from adsorption/desorption isotherms of nitrogen, which were obtained at −196 °C on an Automatic Volumetric Sorption Analyzer (Autosorb-1, Quantachrome). Prior to the determination of the adsorption isotherms, the samples were evacuated overnight at 430 °C under 1.0×10^{-6} mbar vacuum.

Transmission electron microscopy (TEM) images were obtained on a JEOL JEM-100CX II microscope with a CeB_6 filament and an accelerating voltage of 120 kV. The TEM samples were prepared by evaporating one drop of a powdered sample-EtOH suspension (after sonication) onto a carbon-coated holey film supported on a 3 mm diameter, 300 mesh copper grid.

2.3. Acidity characterization (ammonia-TPD and isopropanol dehydration)

The number and acid strength distribution of the active sites were evaluated by temperature programmed desorption (TPD) of ammonia. Experiments were performed on an Altamira AMI-1 instrument consisting of a U-shaped quartz micro-reactor, heated in a vertical furnace. An on-line Baltzers Omnistar mass spectrometer (MS) was used as the detector. Typically, ~0.1 g of sample was placed in the reactor and was thermally treated at 530 °C for 2 h under a helium flow (50 ml min^{-1}). The sample was then cooled to 100 °C and a 5 mol% NH_3/He mixture was used to adsorb ammonia onto the sample for 1 h at this temperature. Prior to desorption, the sample was flushed with flowing helium (50 ml min^{-1}) at 100 °C for 16 h in order to ensure complete removal of physisorbed ammonia. Desorption of ammonia was then carried out from 100 to 700 °C under flowing helium (50 ml min^{-1}) using a temperature ramp of 10 °C min^{-1}. All the desorbed gases were continuously monitored by the on-line MS. In order to calibrate

the MS response to ammonia, a series of 10 constant volume injections of the 5 mol% NH_3/He mixture was performed after the completion of each experiment. Different mass fractions were monitored for desorbed ammonia, water, oxygen, nitrogen, hydrogen and helium. The most abundant mass fractions of ammonia are m/e = 17 and 16. However, determination of ammonia from these two peaks is problematic since they are masked by water usually originating from framework dehydroxylation of the samples. Hence the peak for mass fraction m/e = 15 was also used for the quantitative measurement of desorbed ammonia. Since the intensity of this peak is relatively low, it was monitored with the more sensitive Channeltron detector of the MS instrument.

Dehydration of isopropanol (IPA) was used as the probe reaction to test the acid catalytic activity of the NAS samples. The catalytic tests were performed in a continuous-flow micro-reactor, similar to that described previously [28,29], which consisted of a silica tube with diameter of 1 cm and a sealed-in quartz frit. The catalyst sample (0.2 g) was placed onto the frit and was pre-treated in situ at 530 °C under a helium flow (50 ml min^{-1}) for 2 h. The reactant gas mixture consisted of an IPA-saturated stream, which was prepared by passing helium at 40 ml min^{-1} through a saturator containing IPA and maintained at 20 °C in a thermostated water-bath. The partial pressure of IPA in the gas mixture was estimated to be 4.37 kPa. Analysis of the exit stream was carried out by injecting 1 ml of the gas stream into a Fisons GC-9130 gas chromatograph equipped with a flame ionization detector (FID). The column used for the analysis was a DB-WAX, 30 m × 0.32 mm, with film thickness 0.5 μm, supplied by J&W Scientific. Samples were taken at different reaction temperatures, in the range of 80–180 °C, at 5 °C intervals, after allowing a 30 min equilibration time at each temperature. The reaction rates at the different temperatures were calculated from the percentage conversion of isopropanol and were used as a measure of the relative acid activity of the samples.

3. Results and discussion

3.1. Compositional and structural characteristics—relative crystallinity (chemical analysis, XRD, FT-IR)

The X-ray amorphous or partially crystalline zeolitic NAS materials studied in the present work were synthesized by decreasing the temperature of a typical hydrothermal synthesis of the ZSM-5 zeolite from 150 to as low as 25 °C, while keeping the synthesis time constant at 72 h [23]. The XRD patterns of the samples NAS-50, NAS-90, NAS-130 (synthesized at 50, 90 and 130 °C, respectively) and of the reference ZSM-5/R zeolite are shown in Fig. 1. The % relative XRD crystallinity data for all the NAS samples, compared to the reference ZSM-5/R zeolite, are listed in Table 1. It is evident from the XRD patterns that for the synthesis mixture and the hydrothermal conditions used for the NAS materials [23], the first Bragg peaks appear at the synthesis temperature of approximately 90 °C and their pattern and 2θ values are similar to those of the diffraction peaks found in the XRD pattern of the reference ZSM-5/R zeolite. The 2θ value of the (0 5 1) diffraction peak of the 2% crystalline sample (NAS-90), of the 62% crystalline sample (NAS-130), and of the reference ZSM-5/R zeolite is at about 23.02 deg, indicating that the evolving crystalline structure formed even at 90 °C resembles closely that of the ZSM-5 zeolite. It can also be clearly seen from the XRD results listed in Table 1 that the % relative crystallinity (RC) increases progressively with increasing synthesis temperature, i.e. from 2% at 90 °C to 77% at 150 °C.

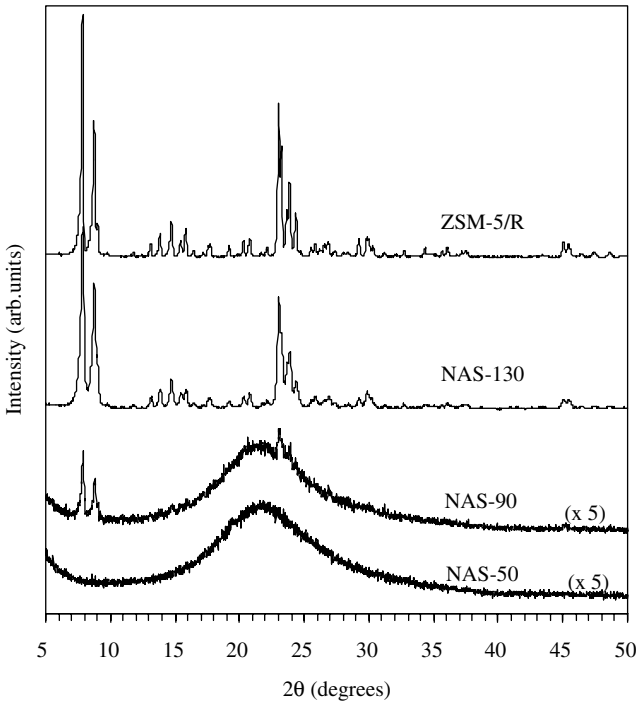

Fig. 1. XRD patterns of the reference ZSM-5/R zeolite and of representative NAS samples with different degrees of crystallinity (the intensity for the samples NAS-50 and NAS-90 is multiplied by 5).

Infrared spectra (IR) spectra of representative NAS samples are shown in Fig. 2. The characteristic band of the five-membered ring of the pentasil structure at ≈547 cm^{-1} can be clearly seen in the spectra of NAS-150 and NAS-130, but it is very small in the case of NAS-110 and hardly identifiable in NAS-90. Although quantification of the IR bands is subject to relatively high % errors, it can be seen that the intensity of the five-membered ring band of the NAS samples increases progressively with increasing synthesis temperature. The estimated % relative crystallinities (RC) based on this IR

Table 1
Chemical composition, relative crystallinity (XRD and FT-IR) and tetrahedral Al (MAS-NMR) of the NAS samples and the reference ZSM-5/R zeolite

Samples	Hydrothermal synthesis temperature (°C)	Chemical composition (wt.%)			Relative crystallinity (%)[a]		Framework Al[b]
		Al	Na	Si/Al	XRD	FT-IR	^{27}Al MAS-NMR ($\times 10^7$)
ZSM-5/R	Commercial	1.40	0.02	28.3	100	100	45.8
NAS-150	150	1.50	0.05	26.7	77	114	39.2
NAS-130	130	1.51	0.02	27.2	62	97	23.2
NAS-110	110	1.54	0.42	27.1	10	14	11.6
NAS-90	90	1.80 (1.78)[c]	1.30 (0.71)	22.8 (22.9)	2	am[d]	11.3
NAS-50	50	1.80 (1.77)	0.68 (0.51)	23.2 (23.5)	am	am	7.2
NAS-25	25	1.58 (1.45)	0.52 (0.40)	26.3 (28.7)	am	am	6.9
AmSiAl	25	1.20	0.09	33.3	am	am	6.6

[a] % Relative XRD crystallinity based on the sum of peak intensities between 22° and 25° 2θ as compared to that of the reference crystalline ZSM-5/R zeolite; % relative FT-IR crystallinity based on the intensity of the peak at 547 cm^{-1} in the IR spectra of the NAS-samples compared to the reference ZSM-5/R zeolite.
[b] Intensity of the individual peak at ~56 ppm in the deconvoluted ^{27}Al MAS NMR spectra of the samples.
[c] The number in parentheses corresponds to wt.% Na and Al after intensive ion-exchange of the samples with NH_4^+, as is described in the experimental section.
[d] Amorphous.

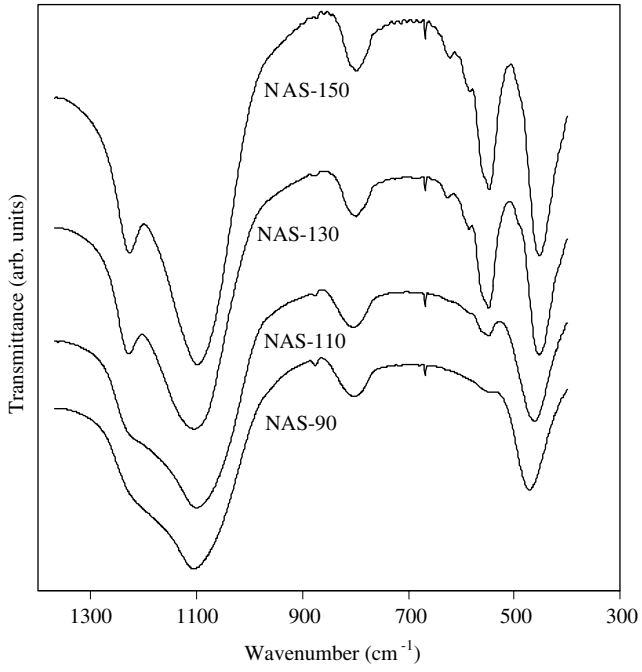

Fig. 2. IR spectra of representative NAS samples with different degrees of crystallinity.

band were considerably higher than the XRD RC for the more crystalline samples, and only small differences were found for the low crystallinity samples (Table 1). Additional evidence for the increase of the framework ordering of the NAS samples that were synthesized at higher temperatures was the progressive development of the peak/shoulder due to the asymmetric stretch vibration of the T–O bond (at ≈1225 cm^{-1}, see Fig. 2), which has been assigned to external linkages (between TO_4 tetrahedra) and is a structure-sensitive IR band [30].

Also listed in Table 1, are the chemical analyses of all the samples studied. It can be seen that the low-crystallinity and X-ray amorphous NAS samples, especially the NAS-90 and NAS-50, have higher aluminum and sodium contents, relative to the high-crystallinity NAS-130 and NAS-150 samples [31]. After intensive and repeated ion-exchange of NAS-90, NAS-50 and NAS-25 with ammonium chloride solutions, as described in the experimental section, the sodium content of these samples decreased but was still higher than that of the highly crystalline samples. The difficulty in removing the sodium from these samples suggests the entrapment of some sodium ions in amorphous oligomeric Si–Al hydroxy-oxides, rather than in zeolitic cation-exchange sites. Furthermore, during this intensive ion-exchange process, some aluminum was leached out from the samples, and especially from NAS-25 (Table 1). It is therefore apparent that some aluminum atoms are present in this sample as soluble salts or hydroxides, which can be easily dissolved at the relatively high ion-exchange temperature of 60 °C that was applied for the repeated ion-exchange experiments.

3.2. Framework aluminum and silicon (^{27}Al and ^{29}Si MAS NMR)

From the ^{27}Al and ^{29}Si solid state MAS NMR experiments evidence was obtained for the improvement in the local symmetry of the tetrahedrally-coordinated aluminum atoms in the framework of the zeolitic precursors and the higher degree of connectivity of the silicon atoms as the hydrothermal synthesis temperature is increased [32]. From the ^{27}Al MAS NMR spectra shown

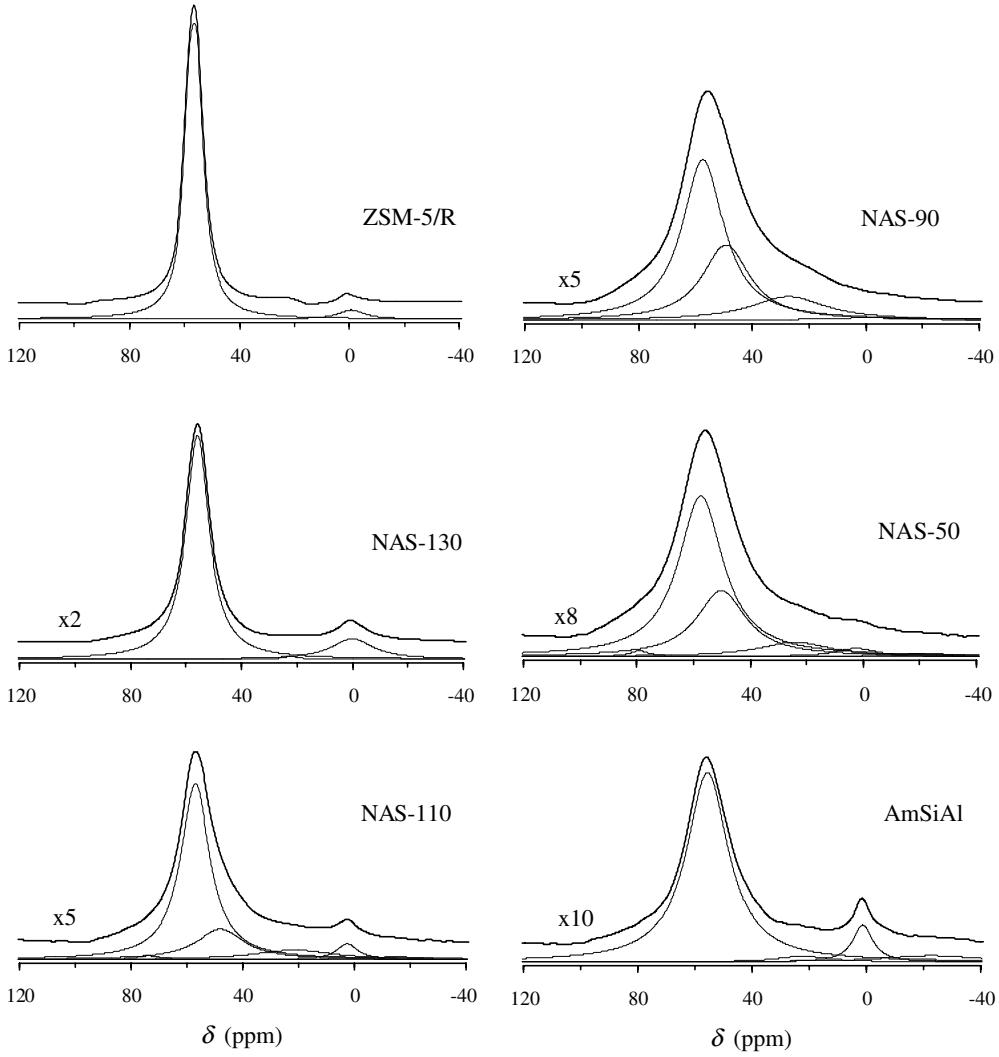

Fig. 3. ^{27}Al MAS NMR spectra of the reference ZSM-5/R zeolite, representative NAS samples and of amorphous silica–alumina: (—) experimental spectra and (---) deconvoluted peaks (the intensity for the samples NAS-130, NAS-110, NAS-90, NAS-50 and AmSiAl is multiplied by 2, 5, 5, 8 and 10, respectively).

in Fig. 3, it can be observed that the resonance at about 55–56 ppm, which in the case of crystalline zeolites is attributed to tetrahedrally coordinated framework aluminum atoms, becomes narrower and more intense for the NAS samples synthesized at higher temperatures and exhibiting higher crystallinities. Similar ^{27}Al MAS NMR data have been previously reported for partially crystalline ZSM-5 samples which were synthesized at constant temperature, i.e. 170 °C, but using shorter synthesis times (6–48 h) [33]. In addition to the resonance at about 55–56 ppm, a very weak signal at about 0 ppm, which corresponds to extra-framework octahedrally coordinated Al species, can also be observed (see Fig. 3), and it is particularly evident in the spectra of the high-crystallinity NAS samples and the reference ZSM-5/R sample. This can be attributed to limited framework dealumination that occurred during the post-synthesis treatments of these crystalline samples (i.e. calcinations to combust the organic template and to produce the H^+-form from the NH_4^+-exchanged samples) [26].

The experimental ^{27}Al MAS NMR spectra of the samples were mathematically deconvoluted using Lorentzian lines (Fig. 3). Apart from the individual deconvoluted peak at about 56 ppm, two other peaks were revealed in the spectra of the low-crystallinity and X-ray amorphous samples. These were a broad one centered at about 25 ppm and a relatively sharp one at about 50 ppm, as can be seen in Fig. 3 for the samples NAS-50, NAS-90 and NAS-110. The relative intensity of these two peaks, compared to the intensity of the peak at about 56 ppm, decreases as the relative crystallinity of the NAS samples increases (NAS-50 to NAS-130). Based on previous ^{27}Al-NMR studies on partially crystalline dealuminated Y and ZSM-5 zeolites [34–39], the peak at about 50 ppm can be attributed to

aluminum species in a distorted tetrahedral environment which progressively transforms into the zeolitic framework as the hydrothermal synthesis temperature increases, while the peak at about 25 ppm can be assigned to five-coordinated extra-framework Al species, mainly present in a less organized extra-framework aluminosilicate phase.

For all the samples studied, the intensities of the individual deconvoluted peak at 56 pmm (Fig. 3), which is attributed to the tetrahedral framework aluminum (FAl) atoms in the zeolitic framework, are listed in Table 1. The relative FAl content of the X-ray amorphous NAS samples is very low as expected, and is not much higher than the tetrahedral aluminum content of the silica–alumina (AmSiAl) sample, and also, does not increase significantly in the low-crystallinity samples, i.e. up to 10% XRD relative crystallinity. Further increase in the value of the relative crystallinity of the samples (i.e. increase of the synthesis temperature) is accompanied by an increase of the FAl content, which becomes only significantly higher at crystallinity levels above 60 %, as can be seen by comparing the peak intensities of the samples NAS-110, NAS-130 and NAS-150 given in Table 1.

In the ^{29}Si MAS NMR spectra of the reference ZSM-5/R zeolite (Fig. 4) there is a well-resolved resonance at about −113.1 ppm with a shoulder at about −116.5 ppm, both corresponding to Si(0Al) units. The relatively broad, low-intensity resonance at about −107.3 ppm is attributed to Si(1Al) units, in accordance with data previously reported for ZSM-5 zeolites [9,32,40]. The framework Si/Al ratio of the reference ZSM-5/R zeolite estimated from the intensities of the above three peaks from the equation $\mathrm{Si/Al} = I_{\mathrm{total}}/0.25I_{\mathrm{Si(1Al)}}$ (where I = peak intensity) was 32.6, which is very close to that determined by chemical analysis (total Si/Al = 28.3). The slightly lower total Si/Al ratio can be attributed to the presence of few extra-framework aluminum atoms, which were also observed in the ^{27}Al NMR spectra as octahedrally coordinated species. The spectra of sample NAS-130 (62% XRD crystallinity) resembles closely that of the reference ZSM-5/R zeolite, except that the intensities of the signals at about −113, −116, and −107 ppm are considerably lower. The framework Si/Al ratio of the zeolitic phase occluded in the partially crystalline sample NAS-130 (62% crystalline) was estimated to be 29.2 (from ^{29}Si MAS NMR), and it was approximately similar to the total Si/Al ratio (27.2). This result indicate a more or less homogeneous distribution of silicon and aluminum atoms between the formed zeolitic phase and the amorphous phases of the sample. The X-ray amorphous NAS-50 sample (synthesized at 50 °C) showed a very weak and broad signal centered at about −111 ppm, which was difficult to deconvolute and was similar to that seen in the spectra of the amorphous silica–alumina sample (Fig. 4).

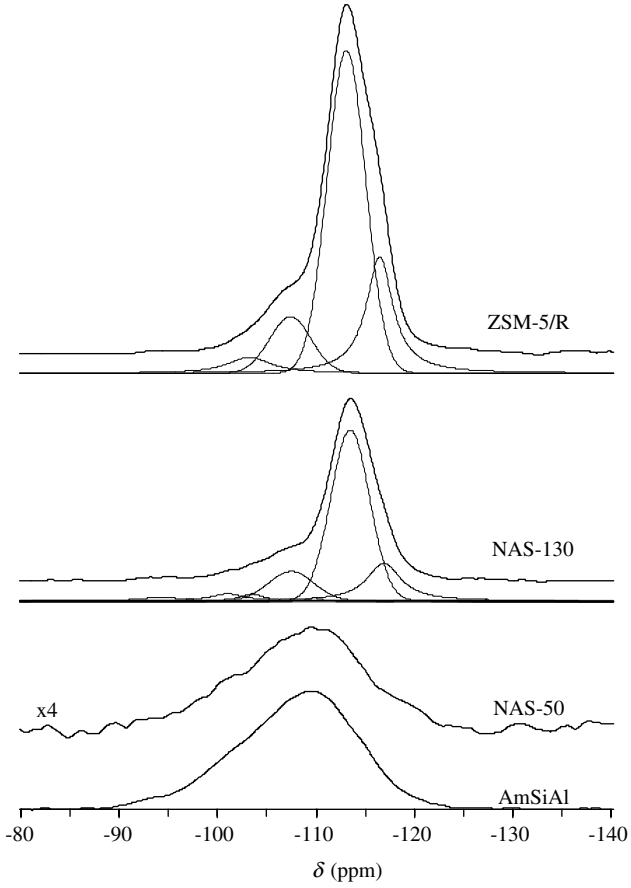

Fig. 4. ^{29}Si MAS NMR spectra of the reference ZSM-5/R zeolite, representative NAS samples and of amorphous silica–alumina: (—) experimental spectra and (---) deconvoluted peaks (the intensity for the sample NAS-50 is multiplied by 4).

3.3. Crystal/particle morphology and porosity characteristics (TEM, N_2 adsorption/ desorption)

The adsorption and porosity characteristics of the NAS samples, the reference ZSM-5/R zeolite and of the amorphous silica–alumina are given in Table 2, and the nitrogen adsorption/desorption isotherms of representative samples are shown in Fig. 5. Although both the micropore area and volume increase with synthesis temperature and % relative XRD crystallinity for all the NAS samples, the total surface area of the amorphous samples NAS-50 and NAS-25 is higher than that of the low-crystallinity sample NAS-90. This is due to the higher macropore and/or external surface area of the amorphous samples as compared to those of NAS-90 (Table 2). Also, the shape of adsorption/desorption isotherms of the amorphous or low-crystallinity samples (Fig. 5) are typical of open surface materials with large meso/macropores ($\geqslant$30 nm diameter from BJH analysis of the desorption isotherm), as well as high external surface areas that allow the formation of multiple adsorbate layers as the P/P_0 increases. On the other hand,

Table 2
Surface area and porosity characteristics of the NAS samples and the reference ZSM-5/R zeolite

Samples	Specific surface area[a] ($m^2 g^{-1}$)	Micro-area[b] ($m^2 g^{-1}$)	Ext + meso/macropore area[b] ($m^2 g^{-1}$)	Micro-pore volume[b] ($cm^3 g^{-1}$)	Total pore volume [c] ($cm^3 g^{-1}$)	Meso + macropore volume ($cm^3 g^{-1}$)
ZSM-5/R	416	339	76	0.141	0.231	0.090
NAS-150	427	338	89	0.144	0.268	0.124
NAS-130	415	304	111	0.134	0.601	0.467
NAS-110	207	90	117	0.041	1.040	0.999
NAS-90	123	33	90	0.014	1.165	1.151
NAS-50	142	28	114	0.011	1.084	1.073
NAS-25	156	26	130	0.010	1.282	1.272
AmSiAl	471	–	471	–	0.661	0.661

[a] Multi-point BET surface area.
[b] *t*-Plot method.
[c] At $P/P_0 \sim 0.99$.

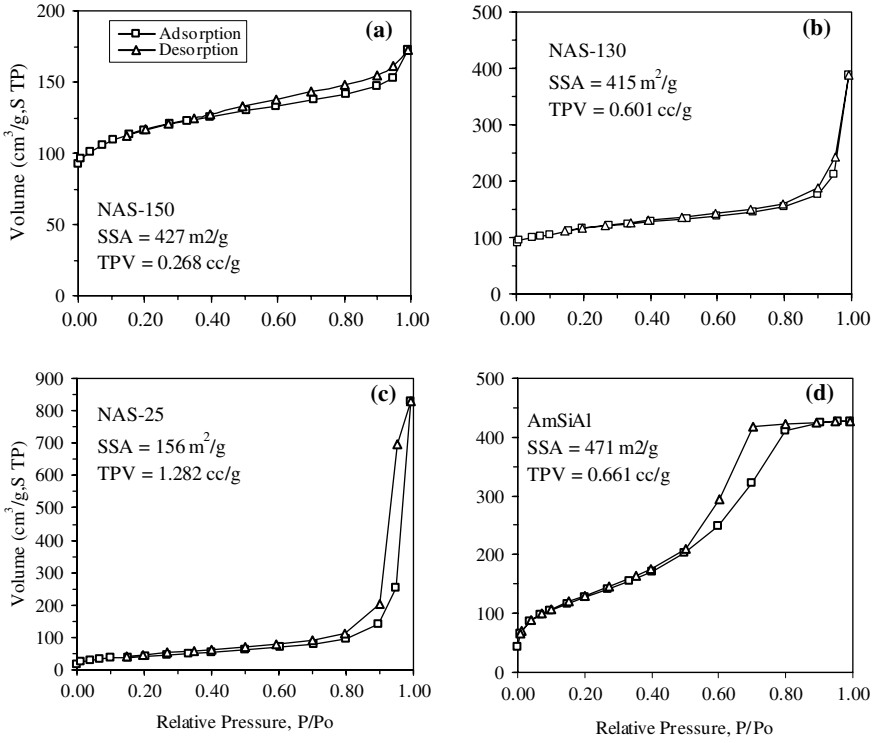

Fig. 5. Nitrogen adsorption/desorption isotherms of representative NAS samples and of amorphous silica–alumina.

the isotherms of amorphous silica–alumina are typical of the relatively ordered mesoporous structures of these aluminosilicates with mean pore diameters of about 6 nm (from BJH analysis of desorption isotherm).

The transmission electron microscopy (TEM) images of the samples are shown in Fig. 6. It can be seen that even the X-ray amorphous samples NAS-25 and NAS-50 consist of small well-formed particles of a nearly spherical shape and dimensions of 20–30 nm. A similar image can be seen for the ~60% crystalline sample NAS-130, except that the particles here are slightly bigger, i.e. 30–50 nm, and are more separated from each other as compared to the relatively more aggregated morphology of the NAS-25 and NAS-50 samples. The high external surface area of the low-crystallinity or amorphous NAS materials can thus be explained by the presence of these small particles which are, however, not small enough or appropriately interconnected in order to generate interparticle ordered mesoporosity, as was previously shown [33]. The particles become larger as the synthesis temperature and the % relative crystallinity increases, reaching the size of the large ZSM-5/R crystals which have a more or less tetragonal or rectangular shape and lateral dimensions of about 300–900 nm (see Fig. 6a). On the other hand, the TEM image of the amorphous silica–alumina (AmSiAl) is typical of a wormhole-like structure with pore sizes of about 5–7 nm, which is in agreement with the results from

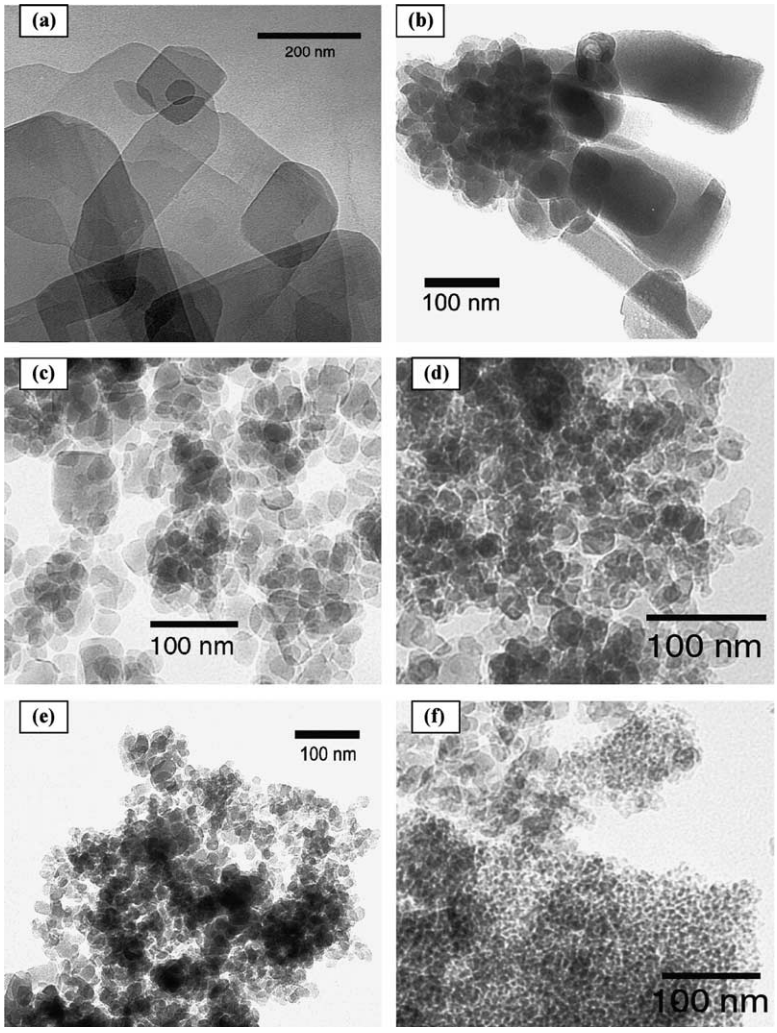

Fig. 6. Transmission electron microscopy (TEM) images of (a) the reference ZSM-5/R zeolite, (b) NAS-150, (c) NAS-130, (d) NAS-50, (e) NAS-25, and (f) amorphous silica–alumina.

nitrogen adsorption/desorption experiments. Some well-formed nanosized particles of spherical shape and with dimensions of around 10–20 nm could also be observed in the images of AmSiAl, but their concentration was very small amongst the particles with typical worm-hole-like structure. Both the X-ray amorphous NAS samples and the amorphous silica–alumina did not give any electron diffraction pattern, whereas with the 2% crystalline NAS-90 sample, some randomly distributed diffraction spots were observed.

3.4. Acidity characteristics—ammonia-TPD

The number and strength of the acid sites were determined by ammonia-TPD measurements. The ammonia-TPD spectra of the H^+-forms of selected NAS-samples and of the reference ZSM-5/R zeolite are shown in Fig. 7. In the spectrum of the H-ZSM-5/R zeolite (which is similar to that of NAS-150), it can be observed that a well-resolved symmetric peak dominates with maximum at about 430 °C, while a shoulder appears at ≈275 °C. Similar NH_3-TPD curves have been previously reported for H-ZSM-5 zeolites, where higher adsorption temperatures (i.e. 150–200 °C) and lower stripping times (1–2 h) were used [41,42]. As the crystallinity of the NAS samples decreases, the main peak becomes smaller and less well-resolved while its maximum also shifts to slightly lower temperatures. The amount of total acid sites, as determined from the areas of the TPD peaks, are listed in Table 3. The experimental TPD curves were further mathematically deconvoluted in order to distinguish between the sites of low/medium and high acid strength, as can be seen in the inset of Fig. 7 for the reference H-ZSM-5/R zeolite. The individual deconvoluted peaks with temperature maxima at about 275 °C and lower were considered as corresponding to sites of low/medium acid strength, while the peaks beyond that temperature were attributed to the relatively strong acid sites.

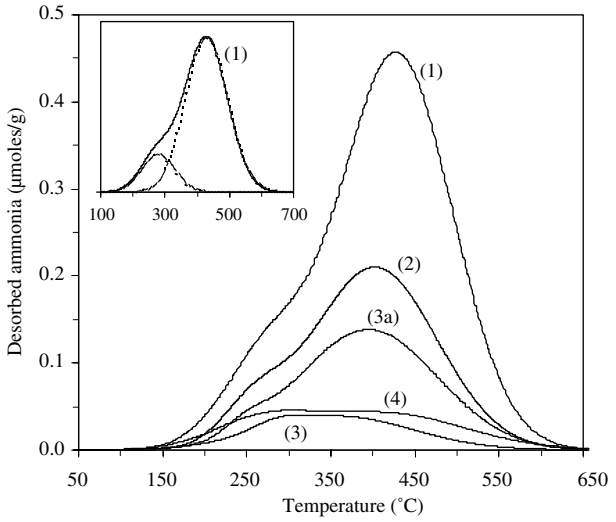

Fig. 7. Ammonia-TPD curves of (1) the reference ZSM-5/R zeolite, (2) NAS-130, (3) NAS-50, (3a) NAS-50 after intensive ion-exchange with NH_4^+, and (4) amorphous silica–alumina. Inset figure: deconvolution of the experimental curve of reference ZSM-5/R zeolite.

Table 3
Acidity characteristics of the NAS samples and the reference ZSM-5/R zeolite

Samples	Total	Number of acid sites (desorbed ammonia) ((mmol/g sample) (±0.01))	
		Weak/medium[a]	Strong
ZSM-5/R	0.54	0.09	0.45
NAS-150	0.53	0.12	0.41
NAS-130	0.27	0.03	0.24
NAS-110	0.15	0.02	0.13
NAS-90	0.02 (0.10)[b]	0.01 (0.01)	0.01 (0.09)
NAS-50	0.05 (0.19)	0.01 (0.01)	0.04 (0.18)
NAS-25	0.10 (0.16)	0.03 (0.03)	0.07 (0.13)
AmSiAl	0.10	0.03	0.07

[a] The weak/medium acid sites correspond to the individual deconvoluted desorption peaks with maxima at about 275 °C and lower, and the strong acid sites to peaks with maxima above that temperature.

[b] The numbers in parentheses refer to the samples that have been intensively ion-exchanged with NH_4^+ ions, as is described in the experimental section.

The number of strong acid sites for the reference highly crystalline H-ZSM-5/R zeolite was 0.45 mmol NH_3 per gram sample, which is very close to its framework aluminum content of 0.46 mmol of Al per gram sample, as determined by the framework Si/Al ratio using the ^{29}Si MAS NMR measurements.

From the data in Table 3, it can also be seen that there is a progressive decrease in the number of total acid sites as the % relative crystallinity of the NAS samples decreases. However, the two X-ray amorphous samples NAS-50 and NAS-25 have a considerably higher number of acid sites compared to the 2% crystalline NAS-90 sample. This unexpected behavior appears to be in contradiction with the higher framework tetrahedral aluminum content of NAS-90 and its higher degree of crystallinity compared to the other two samples. Furthermore, NAS-90 has a disproportionately very low number of acid sites compared to the NAS-110 and the other high crystallinity samples. However, as is shown in Table 1, the sodium content of NAS-90 is significantly higher than that of NAS-50 and NAS-25, and furthermore, in all these three samples, the amount of sodium is considerably higher as compared to the more crystalline samples. When the sodium content of NAS-25, NAS-50 and NAS-90 was lowered through repeated ion-exchange experiments, the number of their acid sites, mainly the strong acid sites, increased markedly (Table 3). This can be clearly seen by comparing the TPD spectra of sample NAS-50 with the spectra of its intensively ion-exchanged counter-part, shown in Fig. 7. It can also be clearly seen from Table 3 and Fig. 7 that the intensively ion-exchanged X-ray amorphous samples NAS-25 and NAS-50 have significantly higher number of strong acid sites compared to the amorphous silica–alumina (AmSiAl) sample, although it was shown that all these samples have similar tetrahedral aluminum contents (^{27}Al NMR results). This could be indicative of the more "zeolitic" character of the tetrahedral aluminum atoms in samples NAS-25 and NAS-50, compared to those of the AmSiAl sample, even though these NAS samples are X-ray amorphous.

3.5. Acid catalytic activity—isopropanol dehydration

The progressive increase of the number of acid sites of the NAS samples with increasing synthesis temperature and % relative XRD crystallinity was also verified by the catalytic results obtained in the dehydration of isopropanol (IPA). The dehydration of low molecular weight alcohol molecules is a typical model reaction for measuring the total acid activity of proton- or alkali-metal exchanged zeolites, since this reaction does not require sites of high acid strength [29,43–45]. An increase of the total number of acid sites results in higher overall rates of IPA dehydration; however, the framework Brønsted acid sites are more active compared to Lewis or Brønsted acid sites generated by alkali cations or extra-framework Si–Al species [29].

Fig. 8 shows the plots of the reaction rates for the total conversion of IPA at different temperatures versus the total number of acid sites of the NAS samples (as measured by ammonia-TPD). From the rate isotherms in Fig. 8 it can be clearly seen that the total conversion of IPA increases as the total number of acid sites of the NAS samples increases. However, it is also evident from the shape of the isotherms that the effect of temperature on the increase of activity is not the same for all the NAS samples. The dehydration rates for the highly crystalline samples NAS-130 (62% crystallinity) and NAS-

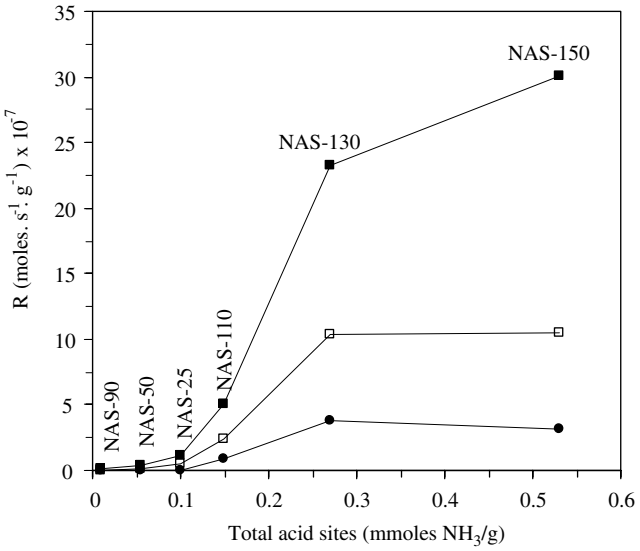

Fig. 8. Reaction rates of isopropanol total conversion versus total number of acid sites of the NAS samples at different reaction temperatures: (●) 100 °C, (□) 110 °C and (■) 120 °C.

150 (77% crystallinity), which have very low content of sodium and extra-framework species and relatively high number of zeolitic Brønsted acid sites, increase significantly from 100 to 120 °C. On the other hand, the activity of the low-crystallinity and X-ray amorphous NAS samples, which have relatively high contents of sodium and extra-framework species and a very low number of zeolitic Brønsted acid sites, is less affected and does not increase significantly in the same temperature range, i.e. from 100 to 120 °C. However, removal of a certain fraction of the sodium ions and extra-framework Al species by intensive ion-exchange, resulted in higher dehydration activities for these samples, in accordance with the increase in the number of their total acid sites (Table 3). Further catalytic studies on these X-ray amorphous and partially crystalline ZSM-5 zeolite-based materials will focus on their capability to be utilized as catalysts or catalyst supports under relatively severe reaction conditions in processes that include continuous reaction-regeneration cycles.

4. Conclusions

The synthesis of X-ray amorphous and partially crystalline nanosized zeolite-based materials can be accomplished by lowering the temperature of a typical hydrothermal synthesis procedure of ZSM-5 zeolite. Small well-shaped spherical particles with dimensions of about 20–30 nm are formed at synthesis temperature as low as 25–50 °C, while the first Bragg peaks are observed with sample NAS-90 (synthesized at 90 °C) and are typical of the ZSM-5 zeolite structure. The micropore area and volume of these nanosized materials increase with the % relative XRD crystallinity while at intermediate degrees of crystallinity they show both microporosity as well as high macropore/external surface area. Incorporation of the aluminum atoms in the ZSM-5 zeolitic framework is significantly enhanced at relatively higher degrees of crystallinity (i.e. at higher synthesis temperatures), for the synthetic route applied in this work. Based on NH_3-TPD and ^{27}Al MAS NMR data it was shown that the X-ray amorphous zeolite-based materials possess tetrahedral aluminum atoms that are more zeolitic in nature and their associated protons are more acidic as compared to those in conventional amorphous silica–alumina. Extensive ion-exchange of the X-ray amorphous and low-crystallinity samples with aqueous solutions of NH_4^+ results in the removal of residual sodium and soluble extra-framework aluminum species that block the strong acid sites of these samples, without any significant changes in their crystallinity and porosity characteristics.

Acknowledgment

The support of the General Secretariat for Research and Technology—Hellas (Project AKMON) is greatly appreciated.

References

[1] J. Scherzer, Catal. Rev.—Sci. Eng. 31 (1989) 215.
[2] A. Humphries, D.H. Harris, P. O'Conner, in: J.S. Magee, M.M. Mitchell Jr. (Eds.), Fluid Catalytic Cracking: Science and Technology, Studies in Surface Science and Catalysis, vol. 76, Elsevier, Amsterdam, 1993, p. 41.
[3] N.Y. Chen, W.E. Garwood, Catal. Rev.—Sci. Eng. 28 (1986) 185.
[4] J.H. Kim, T. Kunieda, M. Niwa, J. Catal. 173 (1998) 433.
[5] J.L. Sotelo, R. Van Grieken, J. Aguado, D.P. Serrano, J.M. Escola, J.M. Menendez, in: M.M.J. Treacey, B.K. Marcus, M.E. Bisher, J.B. Higgins (Eds.), Proceedings of 12th International Zeolite Conference, vol. II, Materials Research Society, Pennsylvania, 1999, p. 1441.
[6] J.P. Gilson, E.G. Derouane, J. Catal. 88 (1984) 538.
[7] M.A. Camblor, A. Corma, S. Valencia, Micropor. Mesopor. Mater. 25 (1998) 59.
[8] C.J.H. Jacobsen, C. Madsen, T.V.W. Janssens, H.J. Jakobsen, J. Skibsted, Micropor. Mesopor. Mater. 39 (2000) 393.
[9] W.P. Zhang, X.H. Bao, X.W. Guo, X.S. Wang, Catal. Lett. 60 (1999) 89.
[10] A.E. Persson, B.J. Schoeman, J. Sterte, J.E. Otterstedt, Zeolites 15 (1995) 611.
[11] M. Tsapatsis, M. Lovallo, T. Okubo, M.E. Davis, M. Sadakata, Chem. Mater. 7 (1995) 1734.
[12] P.A. Jacobs, E.G. Derouane, J. Weitkamp, J. Chem. Soc. Chem. Commun. (1981) 591.
[13] C.E.A. Kirschhock, R. Ravishankar, F. Verspeurt, P.J. Grobet, P.A. Jacobs, J.A. Martens, J. Phys. Chem. B 103 (1999) 4965.
[14] J.C. Jansen, F.J. Van der Gaag, H. Van Bekkum, Zeolites 4 (1984) 369.
[15] M.J. Verhoef, P.J. Kooyman, J.C. Van der Waal, M.S. Rigutto, J.A. Peters, H. Van Bekkum, Chem. Mater. 13 (2001) 683.

[16] R. Ravishankar, C.E.A. Kirschhock, P.P. Knops-Gerrits, E.J.P. Feijen, P.J. Grobet, P. Vanoppen, F.C. De Schryver, G. Miehe, H. Fuess, B.J. Schoeman, P.A. Jacobs, J.A. Martens, J. Phys. Chem. B 103 (1999) 4960.
[17] C.E.A. Kirschhock, R. Ravishankar, L. Van Looveren, P.A. Jacobs, J.A. Martens, J. Phys. Chem. B 103 (1999) 4972.
[18] C.E.A. Kirschhock, R. Ravishankar, P.A. Jacobs, J.A. Martens, J. Phys. Chem. B 103 (1999) 11021.
[19] P.-P.E.A. De Moor, T.P.M. Beelen, R.A. Van Santen, J. Phys. Chem. B 103 (1999) 1639.
[20] P.-P.E.A. De Moor, T.P.M. Beelen, R.A. Van Santen, K. Tsuji, M.E. Davis, Chem. Mater. 11 (1999) 36.
[21] B.J. Schoeman, O. Regev, Zeolites 17 (1996) 447.
[22] Y. Liu, T.J. Pinnavaia, J. Mater. Chem. 12 (2002) 3179.
[23] C.P. Nicolaides, Appl. Catal. A: General 185 (1999) 211.
[24] C.P. Nicolaides, N.P. Sincadu, M.S. Scurrell, Catal. Today 71 (2002) 429.
[25] C.P. Nicolaides, H.H. Kung, N.P. Makgoba, N.P. Sincadu, M.S. Scurrell, Appl. Catal. A: General 223 (2002) 29.
[26] C.S. Triantafillidis, A.G. Vlessidis, L. Nalbandian, N.P. Evmiridis, Micropor. Mesopor. Mater. 47 (2001) 369.
[27] J. Heveling, C.P. Nicolaides, M.S. Scurrell, Appl. Catal. A: General 173 (1998) 1.
[28] A.K. Ladavos, P.N. Trikalitis, P.J. Pomonis, J. Mol. Catal. A—Chem. 106 (1996) 241.
[29] C.S. Triantafillidis, N.P. Evmiridis, Ind. Eng. Chem. Res. 39 (2000) 3233.
[30] E.M. Flanigen, H. Khatami, H.A. Szymanski, Infrared structural studies of zeolite frameworks, in: E.M. Flanigen, L.B. Sand (Eds.), Advances in Chemistry Series, American Chemical Society, Washington, DC, 1971, p. 201.
[31] T.A.J. Hardenberg, L. Mertens, P. Mesman, H.C. Muller, C.P. Nicolaides, Zeolites 12 (1992) 685.
[32] G. Engelhardt, D. Michel, High-Resolution Solid-State NMR of Silicates and Zeolites, Wiley, Chichester, 1987, pp. 106–330.
[33] R. Van Grieken, J.L. Sotelo, J.M. Menendez, J.A. Melero, Micropor. Mesopor. Mater. 39 (2000) 135.
[34] C.A. Fyfe, J.L. Bretherton, L.Y. Lam, J. Am. Chem. Soc. 123 (2001) 5285.
[35] A. Samoson, E. Lippmaa, G. Engelhardt, U. Lohse, H.G. Jerschkewitz, Chem. Phys. Lett. 134 (1987) 589.
[36] M.L. Occelli, M. Kalwei, A. Wolker, H. Eckert, A. Auroux, S.A.C. Gould, J. Catal. 196 (2000) 134.
[37] C.S. Triantafillidis, A.G. Vlessidis, N.P. Evmiridis, Ind. Eng. Chem. Res. 39 (2000) 307.
[38] E. Brunner, H. Ernst, D. Freude, T. Froehlich, M. Hunger, H. Pfeifer, J. Catal. 127 (1991) 34.
[39] A. Maijanen, E.G. Derouane, J.B. Nagy, Appl. Surf. Sci. 75 (1994) 204.
[40] J.B. Nagy, Z. Gabelica, E.G. Derouane, P.A. Jacobs, Chem. Lett. (1982) 2003.
[41] H.G. Karge, L.C. Jozefowicz, in: J. Weitkamp, H.G. Karge, H. Pfeifer, W. Holderich (Eds.), Zeolites and Related Microporous Materials: State of the Art 1994, Studies in Surface Science and Catalysis, vol. 84, Elsevier, Amsterdam, 1994, p. 685.
[42] S.B. Sharma, B.L. Meyers, D.T. Chen, J. Miller, J.A. Dumesic, Appl. Catal. A: General 102 (1993) 253.
[43] P.A. Jacobs, M. Tielen, J.B. Uytterhoeven, J. Catal. 50 (1977) 98.
[44] C. Williams, M.A. Makarova, L.V. Malysheva, E. Paukstis, K.I. Zamaraev, J.M. Thomas, J. Chem. Soc., Faraday Trans. 86 (1990) 3473.
[45] M. Hunger, Catal. Rev.—Sci. Eng. 39 (1997) 345.